Talanta 118 (2014) 339–347

Contents lists available at ScienceDirect

Talanta

journal homepage: www.elsevier.com/locate/talanta

DNA-templated Ag nanoclusters as fluorescent probes for sensing and intracellular imaging of hydroxyl radicals

Li Zhang [a], Ru-Ping Liang [a], Sai-Jin Xiao [b], Jian-Mei Bai [a], Lin-Ling Zheng [c], Lei Zhan [c], Xi-Juan Zhao [c], Jian-Ding Qiu [a,*], Cheng-Zhi Huang [c,**]

[a] Department of Chemistry, Nanchang University, Nanchang 330031, China
[b] Jiangxi Key Laboratory of Mass Spectrometry and Instrumentation, East China Institute of Technology, Nanchang 330013, China
[c] Education Ministry Key Laboratory on Luminescence and Real-Time Analysis, College of Pharmaceutical Science, College of Chemistry and Chemical Engineering, Southwest University, Chongqing 400715, China

ARTICLE INFO

Article history:
Received 8 June 2013
Received in revised form
7 September 2013
Accepted 16 September 2013
Available online 3 October 2013

Keywords:
Ag nanoclusters
Fluorescent probe
Hydroxyl radicals
Intracellular imaging

ABSTRACT

We have developed a simple, rapid and label-free sensor for the essential biological OH• radicals based on the fluorescence quenching of DNA-templated Ag nanoclusters (DNA-Ag NCs). The OH• radicals generated from the Fenton reagent attack and cleave the DNA template, which disturbs the micro-environments around Ag NCs, resulting in spontaneous aggregation due to the lack of stabilization and further the quenching of the Ag NCs fluorescence. These changes in fluorescence intensity allow sensing of OH• radicals with good sensitivity and selectivity under optimal conditions. The sensor can be also applied for quantifying the radical scavenging action of antioxidants. Various characterizations including absorption spectra, fluorescence lifetimes, light scattering (LS) spectra, transmission electron microscopy (TEM), dark field light scattering imaging, and circular dichroism (CD) spectrometry have been employed to illustrate the proposed sensing mechanism. Further investigations demonstrate that the fluorescent probe could penetrate into intact cell membranes to selectively detect intracellular OH• radicals induced by the phorbol myristate acetate (PMA) stimulation. These advantageous characteristics make the fluorescent DNA-Ag NCs potentially useful as a new candidate to monitor OH• in broad biosystems.

1. Introduction

It is known that the redox reactions controlled by a complex enzymatic mechanism in mitochondria would generate radical and nonradical reactive oxygen species (ROS), i.e., superoxide anion ($O_2^{\bullet -}$), hydroxyl radical (OH•), singlet oxygen ($^1O_2$), and hydrogen peroxide (H_2O_2) [1,2]. These oxygen-derived species have been implicated as damaging agents involved in many physiological and pathological conditions, including carcinogenesis [3], inflammatory response [4], ischemia-reperfusion injury [5], and eukaryotic signal transduction [6]. In addition, the accumulation of ROS can lead to alteration of cellular functions responsible for cardiovascular diseases, neurodegenerative diseases, diabetes, cancer, joint diseases as well as aging [7–12]. In particular, the OH• radical produced by the Fenton and Habber-Weiss reactions of H_2O_2 is considered the most aggressive free radical primarily responsible for cellular disorders and cytotoxic effects that can be traced back to the oxidative damage of DNA [13], RNA [14], proteins [15], or lipids [16].

OH• radicals could be monitored using various methods, including electron spin resonance (ESR) [17], high pressure liquid chromatography (HPLC) [18], electrochemistry [19], UV–vis [20], fluorescence [21,22], and luminescence spectroscopies [23]. Although the ESR method using spin trapping agents is a major technique that is currently used for detecting OH•, the method cannot be applied to the real time imaging of OH• in living cells due to the low space resolution. Furthermore, the ESR method requires expensive instrumentation, is laborious, and may involve a number of transient radicals. On the other hand, fluorescence spectroscopy could circumvent many of the shortcomings with respect to inexpensive equipment, easy operation, high selectivity and sensitivity, good reproducibility, and high spatial resolution in imaging techniques [24]. In recent years, there have been some research efforts toward the development of fluorescent probes for evaluating the characteristics of OH•-related biological processes [25]. For example, coumarin derivatives such as coumarin 3-carboxylic acid (C3C), succinimidyl ester of C3C (SECCA), phospholipid-linked coumarins, and coumarin–cyanine hybrid have been used for detection of OH• [26–29]. Tang and co-workers recently designed a new fluorescent probe by covalently combining boron dipyrromethene (BDP) with 2,2,6,6-tetramethyl-1-piperidinoxyl (TEMPO) for the detection of OH• and further the imaging of OH• in mice macrophages [30].

* Corresponding author. Tel.: +86 791 83969518.
** Corresponding author. Tel.: +86 23 68254659; fax: +86 23 68367257.
E-mail addresses: jdqiu@ncu.edu.cn (J.-D. Qiu), chengzhi@swu.edu.cn (C.-Z. Huang).

0039-9140/$ - see front matter © 2013 Elsevier B.V. All rights reserved.
http://dx.doi.org/10.1016/j.talanta.2013.09.021

Although the organic fluorescent probes with good photostability and low cytotoxicity have been widely applied to the $OH^{\bullet}$ sensing, most of them suffer complex synthetic route, time-consuming purification and structure characterizations. In addition, some organic fluorescent probes demonstrate poor solubility, small Stokes shift and relatively low fluorescence quantum yield.

More recently, traditional organic fluorophores are replaced with burgeoning fluorescent nanoparticles such as semiconductor quantum dots, graphene quantum dots, and noble metal nanoclusters. In particular, Ag nanoclusters (Ag NCs), on the order of the de Broglie wavelength of the Fermi level, are known to show discrete, size-tunable electronic transitions and a strong fluorescence emission due to the strong quantum-confinement effect [31,32], which have been applied to the sensing of ions [33,34], small biological molecules [35,36], and biomacromolecules [37,38]. Thus far, a manifold of Ag NCs have been successfully synthesized by the reduction of silver salts in the presence of varying templates, such as poly(amidoamine) dendrimers [39], poly(acrylic acid) derivatives [40], poly(methacrylic acid) [41], peptides [42], protein [43], or DNA [44]. Among the various species investigated so far, Ag NCs encapsulated by the single-stranded DNA through the presence of Ag–Ag bonds and Ag–N/O ligations to DNA arguably constitute the most promising system thanks to their excellent photostability, strong antibunching, good biocompatibility and size tunable optical properties [45].

Since the electronic and optical properties of Ag NCs depend strongly on the nature of the template and of the metal–ligand interaction, the spectral characteristics of DNA-templated Ag NCs (DNA-Ag NCs) can be controlled by the base sequence and DNA length that host the silver atoms, a result that may ultimately contribute to the achieving sequence/length-programmed optical tuning and further constructing turn-on/turn-off fluorescence sensing platform. For example, based on the phenomenon that the red fluorescence of DNA-Ag NCs can be enhanced 500-fold when placed in proximity to guanine-rich DNA sequences, Werner *et al.* designed a "NanoCluster Beacon" for the sensitive hybridization detection in a separation-free format [46]. Moreover, Wang and co-workers demonstrated that the hybridized DNA duplex with an inserted cytosine loop could be employed as capping scaffolds for the generation of fluorescent Ag NCs, and the fluorescence signatures arised from perturbed base pairing in regions adjacent to the cluster template (cytosine loop) could be utilized to identify single-nucleotide mutation [47]. Obviously, in the appropriate context, the susceptible fluorescence conversion of Ag NCs can be used as new signal transduction mechanisms for molecular sensing.

Herein, inspired by the template-dependent properties of DNA-Ag NCs and oxidative damage of template DNA trigged by $OH^{\bullet}$, we demonstrated a novel fluorescence assay for monitoring $OH^{\bullet}$ that was not only sensitive and specific, but also simple and economic in operation (see Scheme 1). We first prepared bright, yellow-emitting Ag NCs by using a template DNA consisting of continuous cytosine bases. In the presence of the $OH^{\bullet}$-generating Fenton reagent, the template DNA is cleaved, which disturbs the microenvironments around Ag NCs, resulting in spontaneous aggregation due to the lack of DNA stabilization and further the quenching of the Ag NCs fluorescence. It was found that the quenching degree proportionably increased with $OH^{\bullet}$ quantity. The strategy can be also used for quantifying the radical scavenging action of antioxidants. Furthermore, the DNA-Ag NCs could penetrate through cell membranes to detect intracellular $OH^{\bullet}$ in human bone marrow neuroblastoma cells. These advantageous characteristics make the fluorescence Ag NCs potentially useful as a new candidate to detect $OH^{\bullet}$ in broad biosystems.

2. Experimental

2.1. Chemicals

Silver nitrate ($AgNO_3$) was purchased from Tianjin Damao Chemical Reagent Co. Ltd. (Tianjin, China); sodium borohydride ($NaBH_4$), vitamin C (ascorbic acid) and ferrous sulfate heptahydrate ($FeSO_4 \cdot 7H_2O$) were obtained from Shanghai Sinopharm Chemical Reagent Co. Ltd. (Shanghai, China). A stock solution (10 mL) of H_2O_2 (0.1 M) was freshly prepared by diluting H_2O_2 (30%, 103 μL) with water, and the concentration was standardized by titration with potassium permanganate. Phorbol myristate acetate (PMA) was purchased from Sigma-Aldrich (USA). All amino acids were obtained from Shanghai Lanji Science and Technology Development Co. Ltd. (Shanghai, China). All DNA strands were purchased from Shanghai Sangon Biological Co. Ltd. (Shanghai, China) and used without further purification. A complete list of DNA sequences used in this study can be found in Table S1 in the ESI†. Oligonucleotides were received as dehydrated pellets and dissolved in sterilized, deionized water. Acetic acid and sodium acetate trihydrate were used to prepare buffers with pH values from 4.4 to 6.0. All other chemicals were from commercial sources and of analytical reagent grade.

2.2. Apparatus

UV–vis absorption spectra were recorded on a Shimadzu UV-2450 spectrophotometer (Tokyo, Japan). Fluorescence spectra as well as light scattering (LS) spectra were performed on a Hitachi F-7000 fluorescence spectrofluorometer (Tokyo, Japan). Fluorescence life time was carried out with a FL-TCSPC fluorescence spectrophotometer (Horiba Jobin Yvon Inc., France). Transmission electron microscopy (TEM) measurements were conducted on a JEM-2010 transmission electron microscope (JEOL Ltd.). Dark field light scattering images were acquired using an Olympus BX51 microscope (Tokyo, Japan) with a high-numerical-aperture dark-field condenser (U-DCW, numerical aperture = 1.2–1.4) for illumination and a 100 × variable-aperture oil immersion objective (UPLANFLN, numerical aperture = 0.6–1.3) for subsequent collection of the scattered light. The dark field images were recorded with a DP72 single-chip color CCD camera (Olympus, Japan). Circular dichroism (CD) spectra were obtained from a Jasco J-810 spectropolarimeter. Fluorescence imaging was performed with an IX81 microscope with a 10 × objective (Olympus, Japan), and the image analysis and processing were performed with Image-Pro® Plus Version 6.3 for Windows™. A QL-901 vortex mixer (Haimen, China) was used to blend the solution.

2.3. Preparation of DNA-Ag NCs

DNA-Ag NCs were prepared using the protocol developed by Ritchie et al. [48]. Briefly, DNA was first dissolved in ultrapure deionized water, then $AgNO_3$ was added into the DNA solution. After the mixture solution was incubated at 4 °C for 1 h, they were reduced with $NaBH_4$ under vigorous shaking for 2 min. The reduced DNA-Ag NCs solution was then kept in the dark overnight at 4 °C. Unless otherwise specified, the final concentrations were 2.5 μM DNA, 15 μM $AgNO_3$, and 15 μM $NaBH_4$. The as-prepared DNA-Ag NCs maintained pale yellow-green solution color and corresponding high fluorescence intensity. To demonstrate the feasibility of our proposed approach, DNA strand 1 containing continuous cytosine bases was chosen as template for the preparation of Ag NCs, which were then employed for $OH^{\bullet}$ sensing. Strands 2–4 were employed as Ag NCs templates to facilitate the sequence investigation, while strand 5 combining PrP^C protein aptamer with continuous cytosine bases was chosen as the

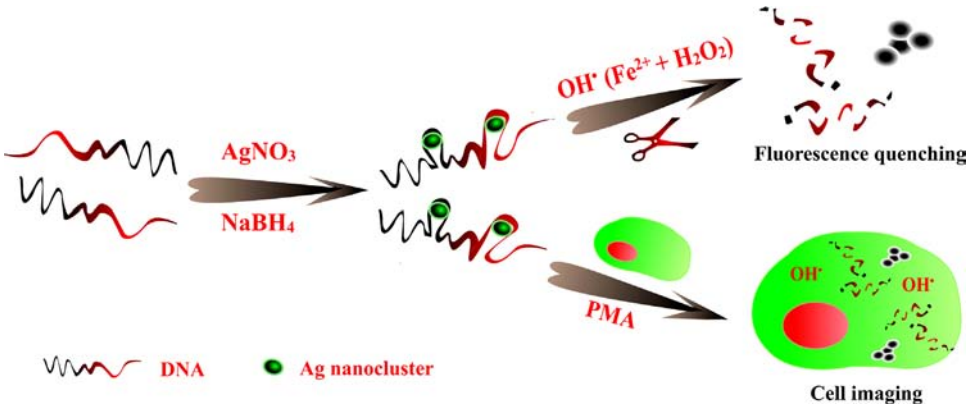

Scheme 1. Schematic representation of the preparation and the operation of DNA-Ag NCs fluorescent probe for the sensing and intracellular imaging of $OH^{\bullet}$ radicals.

template of Ag NCs with orange emission, which could be further utilized for intracelluar $OH^{\bullet}$ imaging.

2.4. DNA-Ag NCs/$OH^{\bullet}$ interaction and scavenger inhibiting procedure

For the sensing of $OH^{\bullet}$, to a 1.5 mL centrifugal tube were sequentially added 40 μL 0.1 M acetate buffer (pH 5.2), 100 μL of the as-prepared Ag NCs solution, 40 μL of 3 mM Fe^{2+} solution, different concentrations of H_2O_2 to generate approximately the expected quantity of $OH^{\bullet}$, and then diluted with deionized water to a final volume of 400 μL. The mixture was then immediately mixed thoroughly on the vortex mixer. After incubation for 5 min, the fluorescence spectra of the resulting solution were recorded upon appropriate excitation wavelength. The resulting solution was further characterized by absorption spectra, fluorescence lifetime, LS spectra, CD spectra, TEM, and dark field light scattering imaging. The inhibition experiment was the same as the above procedure, except for involvement of different amounts of vitamin C in the reaction solution before 20 μL of 100 μM H_2O_2 was added.

2.5. Cell culture and fluorescence imaging

In a typical experiment, human bone marrow neuroblastoma (SK-N-SH) cells were cultured in medium supplemented with 10% fetal bovine serum (FBS) at 37 °C under 5% CO_2, which were then cleaved by trypsin and replaced onto 18 mm glass coverslips in a 24-well tissue culture plate and allowed to grow for 24 h. The medium was then changed with 300 μL of fresh minimum essential medium (MEM, 10% FBS) containing appropriate amounts of DNA-Ag NCs fluorescent probes, and the cells were allowed to grow for another 3 h. A set of cells were stimulated with phorbol myristate acetate (PMA) (200 ng mL^{-1}; a stimulator of cell respiratory burst to give rise to $OH^{\bullet}$) at 37 °C for 5 h. Cells were washed three times with PBS buffer, fixed with 4% paraformaldehyde for 30 min, and sealed with a small amount of glycerol. All background parameters (the laser intensity, exposure time, objective lens) were stationary when the different fluorescence images were captured.

2.6. Cell extracts

The procedure was performed according to Tang et al. with some mofication [21]. The SK-N-SH cells were cultured in medium supplemented with 10% fetal bovine serum (FBS) at 37 °C under 5% CO_2, which were then cleaved by trypsin, and the concentration was counted to be 1×10^6 cells mL^{-1}. Appropriate amounts of DNA-Ag NCs fluorescent probes were added and incubated at 37 °C for 3 h. A set of cells were stimulated with PMA (200 ng mL^{-1}) at 37 °C for 5 h. All cells were harvested by centrifugation, and then washed three times with PBS buffer. The cells were then disrupted for 10 min in a GA88-Π ultrasonic disintegrator. The broken cell suspension was centrifuged at 6000 rpm for 15 min, and the pellet was discarded. The PMA-stimulated cell supernatant solutions were analyzed by the proposed method as well as the standard HPLC method [18]. For the recovery studies, the PMA-stimulated cells suspension was divided into twelve parts, and standard solution of Fe^{2+} (0.3 mM)/H_2O_2 (0.5 μM) were added into six parts in turn.

3. Results and discussion

3.1. Optical characterization of DNA-Ag NCs

The UV–vis absorption spectrum of an aqueous solution of the in situ formed DNA-Ag NCs shows a narrow maximum of λ_{max}=397 nm and broad bands characterized at 433 and 550 nm (Fig. S1-A in the Supporting Information). The three electronic transitions were all considered indicative of genuine small nanoclusters, in particular Ag_2 and Ag_3 [49], as expected from theoretical and low-temperature spectroscopic studies. Thus far, a definitive assignment of the electronic bands is problematic on the basis of these prior studies because the peaks for the DNA-Ag NCs are expected to shift and broaden relative to their gas phase and rare gas matrix-isolated values [44].

As opposed to larger Ag nanoparticles, a distinctive feature of Ag NCs is their strong fluorescence due to their lower density of electronic states. For the DNA-Ag NCs, several electronic transitions were observed-one prominent band with maximum emission at 550 nm (λ_{em}=550 nm) upon 440 nm excitation (λ_{ex}=440 nm) and two weaker bands with λ_{ex}=280 nm/λ_{em}=620 nm and λ_{ex}=550 nm/λ_{em}=612 nm (Fig. S1-A, B). It was worth noting that the transition band with 280 nm excitation has a similar emission wavelength to that with 550 nm excitation, which suggests that the nanocluster emission may occur *via* energy transfer, the nanoclusters also have higher lying excited states accessible in this spectral region [44], and thus emission following direct excitation of the higher electronic bands of the Ag NCs is also feasible. Furthermore, it was observed that excitation at wavelengths greater than 530 nm results in red-shifts of the λ_{em} with increasing λ_{ex} (Fig. S1-C), a result that was observed in previous studies [44], demonstrating that at least two distinct species contribute to the fluorescence in this wavelength region. The multiple transition bands in both the absorption and fluorescence spectra provide sufficient evidence that the Ag NCs samples contain multiple species with varying stoichiometries, and the maximum fluorescence spectrum with λ_{ex}=440 nm/λ_{em}=550 nm

was utilized in the following experiment to evaluate the effect of $OH^{\bullet}$ on the fluorescence emission of DNA-Ag NCs.

3.2. Interaction of DNA-Ag NCs with $OH^{\bullet}$ radicals and antioxidation investigation

The fluorescence assay for $OH^{\bullet}$ radicals was performed by using Fenton's reagent. It is well known that $OH^{\bullet}$ can be generated by the Fenton reaction in which Fe^{2+} reacts with H_2O_2, thereby producing the $OH^{\bullet}$ and $FeOH^{2+}$ (Eq. 1).

$$Fe^{2+} + H_2O_2 \rightarrow FeOH^{2+} + OH^{\bullet} \quad (1)$$

The generated $OH^{\bullet}$ can cleave the DNA strand into different sequence fragments and even single bases by abstracting a hydrogen atom from a deoxyribose sugar in the DNA backbone [50]. Inspired by the fact that the fluorescence intensity of DNA-Ag NCs depends on base sequence and conformation, a straightforward strategy for $OH^{\bullet}$ sensing has been explored based on the cleavage of template DNA.

The mechanism of our novel fluorescence nanosensor is shown in Scheme 1, and the fluorescence spectra of Ag NCs in the presence of different concentrations of $OH^{\bullet}$ are demonstrated in Fig. 1A. In this experiment, the concentration of $OH^{\bullet}$ was changed by changing the concentration of H_2O_2, as described in the experimental section. When H_2O_2 and Fe^{2+} were added separately, the fluorescence intensity (λ_{ex}=440 nm/λ_{em}=550 nm) of Ag NCs showed no significant change. Only when H_2O_2 and Fe^{2+} were added simultaneously, was a remarkable decrease in fluorescence intensity found due to the formation of $OH^{\bullet}$. If the Ag NCs and Fe^{2+} concentrations were held constant, then the fluorescence intensity of Ag NCs linearly decreased with an increase in concentration of H_2O_2. The Stern–Volmer plot showed a linear relationship (R^2=0.9922) between the fluorescence decrease with the concentration of H_2O_2 over the range from 50 nM to 5.0 μM (Fig. 1B), demonstrating the $OH^{\bullet}$-dependent oxidative/cleavage efficiency. Interestingly, the other emission band (λ_{em}=612 nm) responded differently to Fenton's reagent, it was found that the addition of 0.3 mM Fe^{2+} could completely quench their fluorescence (data not shown), and the reason might be explained as follows: since the Fe^{2+} would be partly oxidized to Fe^{3+} with the involvement of dissolved oxygen under our experimental conditions, where the small amount of Fe^{3+} as relatively strong oxidizer could react with the reduced species associated with the λ_{ex}=550 nm/λ_{em}=612 nm bands [48], and thus efficiently quench its fluorescence. In view of the intensive quenching of the fluorescence emission (λ_{em}=550 nm) of DNA-Ag NCs in the presence of $OH^{\bullet}$, it was possible to develop a new Ag NCs-based fluorescence sensing system for $OH^{\bullet}$.

This new approach to quantify the action of free radicals by their destruction of DNA template can be also applied for quantification of antioxidants, that is, scavengers of free radicals. This process is shown by the addition of ascorbic acid to the Fenton solution [19], which leads to an easily detectable decrease of the destructive power of the Fenton solution, reflected in the fluorescence recovering with increasing ascorbic acid concentration (Fig. 2). Hence, our novel strategy can not only efficiently probe the $OH^{\bullet}$ through the fluorescence quenching of Ag NCs triggered by the breakage of DNA template, but also provide a rapid and convenient method to screen antioxidation natural products or drugs.

3.3. Optimization of interaction conditions

To obtain the optimal experimental conditions for the proposed method, we first explored the effect of pH on the fluorescence intensities of Ag NCs in the absence and presence of $OH^{\bullet}$. Since Ag NCs bind preferentially with the N3 of the cytosine base, it is expected that the increase of pH values higher than the p*K*a of the N3 of cytosine (4.5) would promote the deprotonation of N3, and thus enhanced the fluorescence intensities due to the elevated nanocluster binding [48]. The experimental results in Fig. S2-A in the Supporting Information demonstrated that the fluorescence intensity of Ag NCs gradually increased with pH from 4.4 to 5.2 and then the tendency became slight with further increase of pH, while the quenching efficiency of fluorescence intensity with $OH^{\bullet}$ reached the maximum around the pH 5.2. At more basic pH values (pH > 5.2), the iron is converted from a hydrated ferrous form to a colloidal ferric form, thereby causing a decrease in the effectiveness of the reaction and further inhibiting the DNA cleavage [51]. In order to ensure a higher fluorescence intensity of the Ag NCs blank and better quenching efficiency between the Ag NCs and $OH^{\bullet}$, a pH value of 5.2 in acetate buffer was employed throughout.

The concentration of Fe^{2+} was also optimized, Fig. S2-B indicates that either in the absence or presence of H_2O_2, the fluorescence intensities of Ag NCs got enhanced slightly with increasing the concentration of Fe^{2+}, while the quenching efficiency almost remained constant over the range of 0.075–0.75 mM, indicating that the excessive Fe^{2+} over this concentration range can hardly affect the $OH^{\bullet}$ generation. To ensure the molar ratio of Fe^{2+}/H_2O_2 higher than 10 for all involved H_2O_2 concentrations, a 0.3 mM Fe^{2+} solution was chosen.

3.4. Investigation of interaction mechanism

The efficient fluorescence quenching of DNA-Ag NCs by $OH^{\bullet}$ raised two important questions. What changes in the Ag NCs morphology and distribution make the fluorescence intensities in the absence of $OH^{\bullet}$ different from those in the presence of $OH^{\bullet}$,

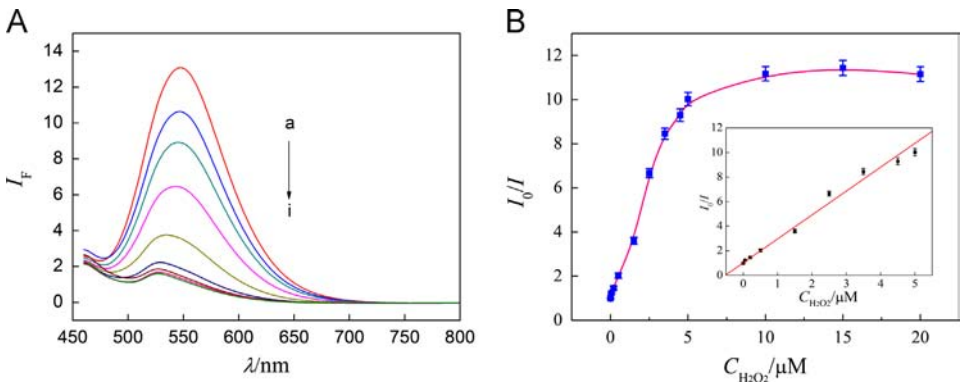

Fig. 1. (A) Fluorescence spectra of DNA-Ag NCs after reaction with $OH^{\bullet}$ (at various H_2O_2 concentrations), the H_2O_2 concentrations were (from a to i): 0, 0.05, 0.2, 0.5, 1.5, 2.5, 3.5, 4.5 and 5.0 μM. (B) Fluorescence responses of DNA-Ag NCs to various concentrations of added H_2O_2 in 0.1 M acetate buffer (pH 5.2) containing 0.3 mM Fe^{2+}.

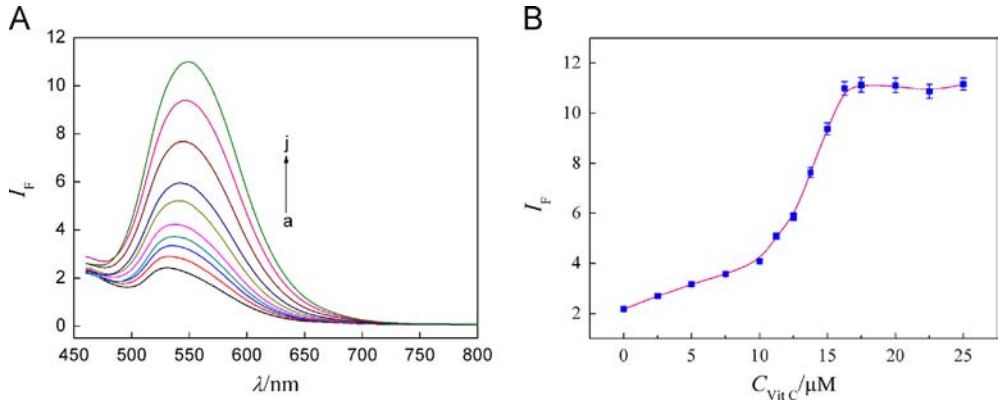

Fig. 2. (A) Fluorescence spectra of DNA-Ag NCs after exposure to Fenton's reagent (0.3 mM Fe^{2+}, 5.0 μM H_2O_2) in the absence or presence of various amounts of vitamin C (ascorbic acid), the vitamin C concentrations were (from a to j): 0, 2.5, 5.0, 7.5, 10.0, 11.25, 12.5, 13.75, 15.0 and16.25 μM. (B) Dependence of the increase of the fluorescence intensity of DNA-Ag NCs after exposure to Fenton's reagent (0.3 mM Fe^{2+}, 5.0 μM H_2O_2) on the concentration of vitamin C.

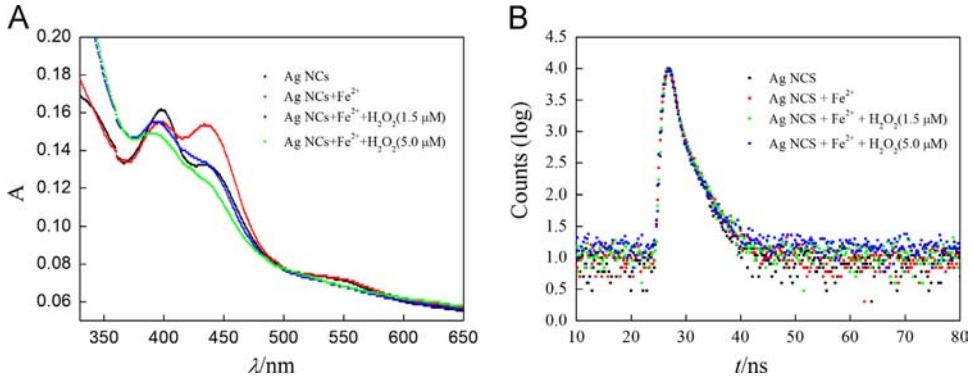

Fig. 3. (A) Absorption spectra of DNA-Ag NCs after reaction with Fenton's reagent. (B) Fluorescence decay as a function of time of DNA-Ag NCs in the presence of Fenton's reagent. (0.1 M pH 5.2 acetate buffer, the concentration of Fe^{2+} was 0.3 mM).

and what structural changes in template DNA are responsible for the distribution evolution of Ag NCs?

In addressing these questions, many aspects of Ag NCs distribution and template DNA structure warrant consideration. Absorption spectra were important in determining nanoparticle species with different electronic transitions. Fig. 3A shows the absorbance curves of DNA-Ag NCs in the presence of Fe^{2+} and H_2O_2. It was found that the shoulder of the peak located at 433 nm remarkably enhanced with the decrease of the maximum band at 397 nm after the addition of Fe^{2+}. The evolution of these absorbance peaks might be assigned to the energy transfer between different species under Fe^{2+} titration [43], and the investigation on detailed mechanism is still in progress. In the presence of H_2O_2, the absorption peak at 433 nm slowly broadened and decreased with increasing H_2O_2 concentration, indicating that the template DNA has been cleaved by the generated $OH^{\bullet}$, and thus the unstable Ag NCs would be released from the capping agent and aggregated to larger nanoparticles, which could be further confirmed by the blue-shift and broadness of the absorption band located at 397 nm. We then performed a series of experiments, including fluorescence lifetimes, LS assay, TEM measurements and dark field light scattering imaging to ensure that the observed fluorescence quenching was due to the Ag NCs aggregation, and employed CD spectrometry to prove that the occurrence of $OH^{\bullet}$-induced DNA scission was responsible for the release of Ag NCs from DNA template.

Lifetime measurements of DNA-Ag NCs in the presence of Fenton's reagent were performed at the emission wavelength of λ_{em}=550 nm. The fluorescence decay curves are shown in Fig. 3B, demonstrating that the fluorescence intensity of DNA-Ag NCs in the absence and presence of $OH^{\bullet}$ decreased over time, and the data followed the triexponential fitting equation:

$$F(t) = A_1 e^{(-t/\tau 1)} + A_2 e^{(-t/\tau 2)} + A_3 e^{(-t/\tau 3)}$$

allowing us to determine the values of lifetime τ_1, τ_2 and τ_3. Since electron charge transfer from Ag to DNA scaffolds occurred in the Ag-DNA complex [52], the triexpoential decay was possibly attributed to the differential distribution of complicated luminescent pathways of polynuclear Ag-DNA complexes [34,53]. The lifetimes of the DNA-Ag NCs are listed in Table S2 in the Supporting Information, revealing that they all followed triexponential decays, with slight differences in the values of A_1, A_2 and A_3 under different conditions. It was found that the lifetime of the DNA-Ag NCs did not obviously change with the addition of different concentrations of $OH^{\bullet}$. The unchanged fluorescence lifetime and linear Stern–Volmer plot (Fig. 1B) imply that the quenching of the Ag NCs by $OH^{\bullet}$ obeyed a simple static quenching mechanism—i.e., the $OH^{\bullet}$ cleaved the template DNA into different sequence fragments and even single bases, and destruction of the DNA strand likely leading to the aggregation of unprotected Ag NCs, and to the subsequent formation of large Ag nanoparticles with non-fluorescence. In other words, the fluorescence quenching was due to the disappearance of bright species with a remaining population of nanoclusters (unaggregated) that were of comparable brightness, ruling out the fluorescence resonance energy transfer (FRET) mechanism since the absorption of DNA does not overlap with the emission spectrum of the Ag NCs (Fig. S3 in the Supporting Information).

To further evaluate the performance and consistency of our assay, we measured the enhanced LS signals of aggregated Ag NCs by scanning synchronously both the excitation and emission

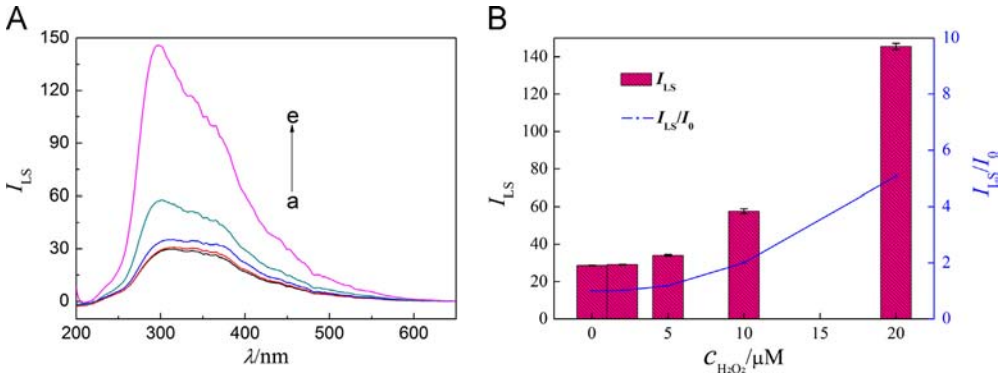

Fig. 4. (A) LS spectra of DNA-Ag NCs after reaction with OH• (at various H_2O_2 concentrations), the H_2O_2 concentrations were (from a to e): 0, 2.0, 5.0, 10.0 and 20.0 μM. (B) LS responses of DNA-Ag NCs as a function of H_2O_2 concentration in 0.1 M acetate buffer (pH 5.2) containing 0.3 mM Fe^{2+}.

monochromators of a common spectrofluorometer. As shown in Fig. 4A, the LS intensity of the solution containing Ag NCs and Fe^{2+} was very weak in the absence of H_2O_2. It was worth noting that the LS would be only Rayleigh scattering because the diameter of the Ag NCs was smaller than 1/20 of the incident wavelengths [54]. Notably, the LS intensity of Ag NCs can be greatly enhanced in the presence of OH• (by introducing H_2O_2) in the wavelength range of 250–500 nm, and the LS spectra maintained almost the same pattern as the concentration of H_2O_2 increased. The enhanced LS intensities as a function of H_2O_2 concentration confirmed the formation of Ag NCs aggregates (Fig. 4B), which were fully consistent with the absorption and lifetime results, and strongly supported our speculations that the fluorescence quenching was ascribed to the Ag NCs aggregation. It should be noticed that the LS assay exhibited lower sensitivity to OH• than the fluorescence method because of the more sensitive responsiveness of fluorescence to the formation of aggregates compared with that of light scattering.

A direct evidence for the aggregation of Ag NCs could further be provided by TEM measurements and dark field light scattering imaging. We note that while a few nanoparticles were larger than 10 nm, the majority of as-prepared DNA-Ag NCs were well-dispersed with the average size smaller than 5 nm (Fig. 5A). Small clusters are known to have a tendency for agglomeration. The prepared DNA-Ag NCs still retained the monodispersed states with key emissive properties, probably due to the intrinsic bond strength in diatomic or triatomic silver and further stabilization by the cytosine-rich DNA. In the presence of OH•, the aggregation species of Ag NCs with the average diameter of 50 nm were formed (Fig. 5B), which was much larger than that of the individual nanoclusters before treatment with OH•. Furthermore, the aggregation process could be verified with the dark-field microscope. As shown in Fig. 5C, because of the low scattering intensity and faster diffusion of the small Ag NCs, the light scattered from single DNA-Ag NCs was not readily observed by our system. Note that strong scattering occurred once the DNA-Ag NCs were treated with OH•, where the bright blue spots in Fig. 5D corresponded to the scattering images of Ag NCs aggregates.

We further employed CD spectrometry to identify the breakage and cleavage of template DNA triggered by OH•. It is well known that the electronic transition of the DNA bases exhibit a small CD due to the chirality of the riboses, and this spectroscopic technique is sensitive to the arrangement of the bases. For the Ag NCs complex with template DNA, CD studies show that Ag NCs induced slight nonplanar and tilted orientations of the bases relative to the normal DNA form (black curve and red curve in Fig. S4), which could be attributed to the alteration of the dipole coupling between the excited electronic states of the bases induced by structural changes after the Ag NCs formation [44]. The addition of Fe^{2+} caused the ellipicity at 248 nm and 278 nm to decrease due to the looser structure of template DNA [55]. As a result, the template DNA became more flexible, enhancing their capping capability for stabilizing the DNA-Ag NCs [56], and thus exhibiting better resistance to the environmental quenching, which was consistent with the experimental results that the fluorescence intensity of DNA-Ag NCs slightly enhanced with Fe^{2+} concentration (Fig. S2-B). Further increasing the H_2O_2 concentration from 0 to 5.0 μM caused the Cotton effect to decrease (Fig. S4). In the presence of 5.0 μM H_2O_2, the fluorescence of DNA-Ag NCs was quenched by greater than 95% (Fig. 1), while both the positive and negative Cotton effect decreased close to that of the pure water, revealing that DNA played an important role in determining the fluorescence of DNA-Ag NCs. When the template DNA was gradually cleaved by OH•, Ag NCs were exposed to the bulk solution to a greater extent, and the degree of quenching, due to aggregation of the nanoclusters, increased.

3.5. Sequence investigation

To further confirm the generality and controllability of the regulation of fluorescence quenching by DNA cleavage, the other three cytosine-rich oligonucleotides, 24mer strand 2, 12mer strand 3 and 12mer strand 4 were chosen as the Ag NCs template, and the sequence details are listed in Table S1 in the Supporting Information. The DNA-Ag NCs synthesis procedure was similar to that for the 42-base strand 1, and the conditions for the DNA-Ag NCs/OH• interaction were the same as that for the 42mer DNA-Ag NCs-participated reaction. As shown in Fig. 6A, the fluorescence responses to a series of OH• concentrations were in accordance with former results except for the blue-shift of the maximum emission wavelength to 515 nm, suggesting that the Fenton reaction was able to induce DNA damage and then quench the fluorescence of Ag NCs despite employing different DNA sequences. In addition, the slopes corresponding to the fluorescence quenching efficiency were found to depend on the template DNA structure-including sequence and length (Fig. 6B). In other words, a shorter template DNA sequence gave rise to a relatively faster cleavage rate, thus the higher fluorescence quenching efficiency of Ag NCs (Fig. 6B, strand 2 and strand 3). In addition, since the DNA damage induced by Fenton's reagent is partially site-specific, where cytosine is the most sensitive of the four bases to Fenton reactions [57], making it more susceptible to oxidative breakage. Therefore, a higher occurrence of DNA damage to strand 3 was obtained in comparison with that of strand 4, resulting in higher fluorescence quenching efficiency.

3.6. Selectivity of the method

The selectivity of DNA-Ag NCs for OH• is very important, especially when the fluorescent probe is applied to cellular systems, and so the effects of interfering species normally found in association with

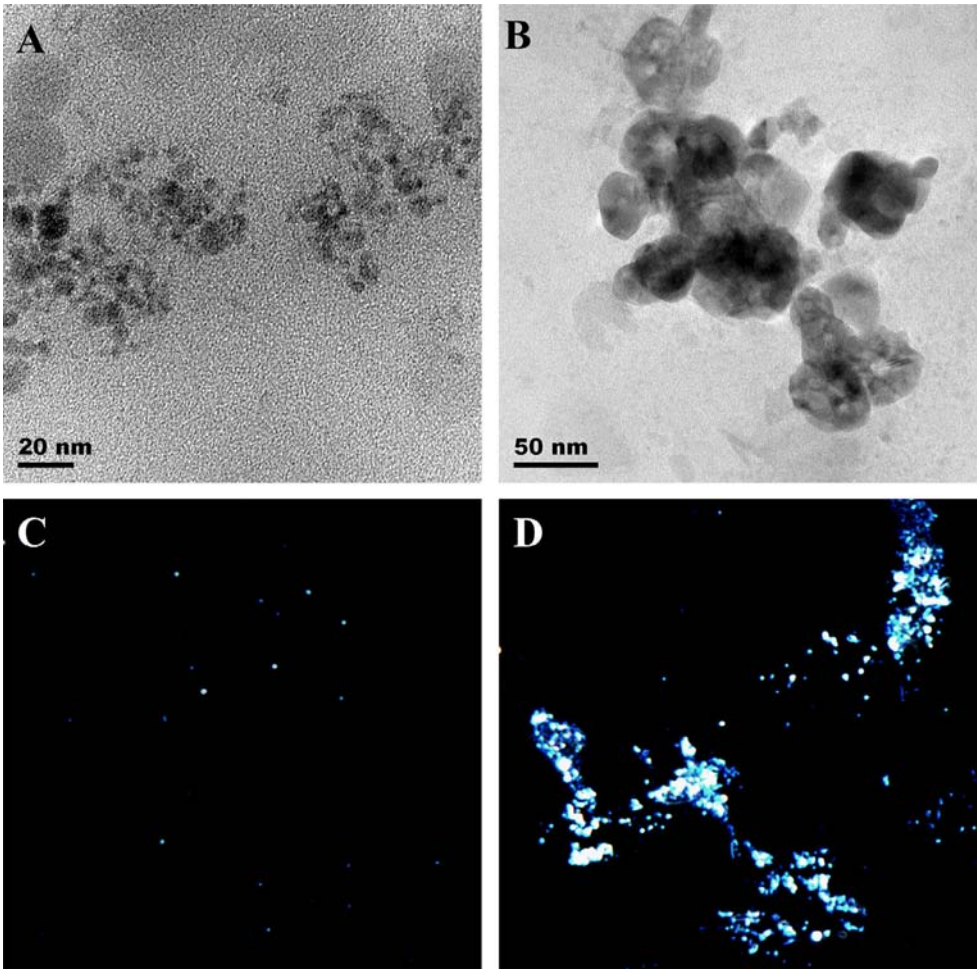

Fig. 5. TEM images (A, B) and dark field light scattering images (C, D) of DNA-Ag NCs in the absence (A, C) and presence of $OH^{\bullet}$. (0.1 M pH 5.2 acetate buffer, the concentration of Fe^{2+} and H_2O_2 was 0.3 mM and 5.0 μM respectively).

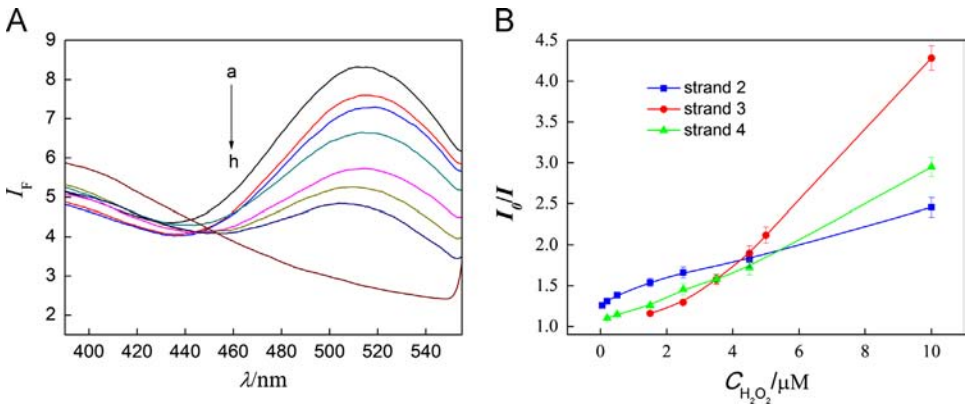

Fig. 6. (A) Fluorescence spectra of DNA-Ag NCs (strand 4) after reaction with $OH^{\bullet}$ (at various H_2O_2 concentrations), the H_2O_2 concentrations were (from a to h): 0, 0.2, 0.5, 1.5, 2.5, 3.5, 4.5 and 6.0 μM; (B) Fluorescence responses of DNA-Ag NCs (strand 2–4) as a function of H_2O_2 concentration in 0.1 M acetate buffer (pH 5.2) containing 0.3 mM Fe^{2+}.

biological system were studied (Fig. 7). The experimental results demonstrated that only $OH^{\bullet}$ induced a dramatic decrease in the fluorescence intensity, whereas neither Fe^{2+} nor H_2O_2 can markedly affect the stability and the fluorescence property of Ag NCs. Moreover, the DNA-Ag NCs showed no significant fluorescence decrease when various cations-such as Na^+, K^+, Ca^{2+}, Mg^{2+}-were added. Other biological compounds such as lysine (Lys), glutamic acid (Glu), serine (Ser), histidine (His) and glucose were also investigated and did not make interferences with the sensing of $OH^{\bullet}$. These observations revealed that the present method provided relatively high selectivity toward $OH^{\bullet}$, which was ascribed to the high-specificity of $OH^{\bullet}$ for DNA cleavage, and allowed its quantitative determination in biological samples.

3.7. *Fluorescence imaging and detection of $OH^{\bullet}$ in cells*

In light of the afore-mentioned favorable properties of DNA-Ag NCs, we proceeded to examine its potential utility for fluorescence

imaging of $OH^{\bullet}$ in living cells. In order to specifically recognize the membrane protein–cellular prion protein (PrP^C) on the SK-N-SH cells, the template DNA used for Ag NCs synthesis has been modified to obtain a new fluorescent recognition ligand that combines the strong fluorescence of DNA-AgNCs with the specificity and strong binding affinity of DNA aptamers for the target proteins PrP^C, and the DNA sequence (strand 5) as well as other details were demonstrated in Section 2. It was found that DNA-Ag NCs could penetrate through the cellular membrane when incubated with the cells at 37 °C and the orange emission was concentrated in the nuclei (Fig. 8A–C). Although the fluorescence intensity might decrease to a certain extent due to the specific interaction between DNA-AgNCs and target membrane protein [37], the remnant intense fluorescence would be adequate for imaging under our experimental conditions. The internalization of these nanoclusters illustrated that DNA-AgNCs served as both a fluorescent label and a specific binding ligand can be potentially applied as a reporter of endocytic uptake and vesicular transport. Further experimental results demonstrated that the cells incubated with phorbol myristate acetate (PMA, a stimulator for production of $OH^{\bullet}$) and DNA-Ag NCs exhibited much weaker fluorescence in the orange channel (Fig. 8D–F) compared with that treated with only DNA-Ag NCs (Fig. 8 A–C), indicating that DNA-Ag NCs, as a selectively cell-permeable probe, can respond to changes in intracellular $OH^{\bullet}$ concentrations.

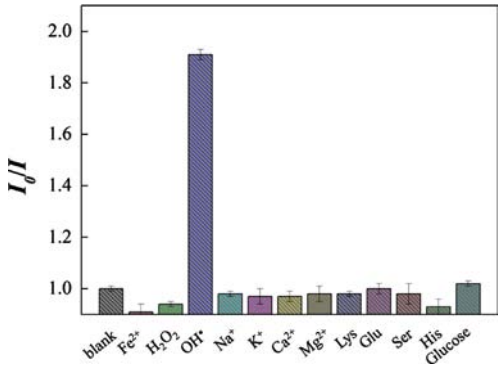

Fig. 7. Fluorescence responses of DNA-Ag NCs to 0.5 μM $OH^{\bullet}$, 0.3 mM Fe^{2+}, and 5.0 μM other various species.

To further investigate the feasibility of the proposed assay in biological systems, determination of $OH^{\bullet}$ in cell extracts was performed. The detected $OH^{\bullet}$ content of PMA-stimulated cell extracts was 0.35 ± 0.04 μM ($n=6$), based on a correlation between the fluorescence intensity of the cell extracts and the regression equation. The value is consistent with the result obtained by the standard HPLC method, i.e., 0.31 ± 0.02 μM ($n=6$). The average recovery test was conducted utilizing the standard addition protocol, and the standard deviation (SD) was obtained from a series of six cell extracts (Table 1). The results demonstrate that the present method could be applied to determine low level of intracelluar $OH^{\bullet}$ with good accuracy and precision.

Table 1
Determination of $OH^{\bullet}$ in cell extracts ($n=6$). PMA, 200 ng mL^{-1}; Fe^{2+} (0.3 mM)/H_2O_2 (0.5 μM).

Sample	$OH^{\bullet}$ content of PMA-stimulated cells (μM)		Added (μM)	Found (μM)	Recovery (%)
	The proposed method	HPLC method			
Cell extracts	0.35 ± 0.04	0.31 ± 0.02	0.5	0.84 ± 0.03	99.0 ± 3.6

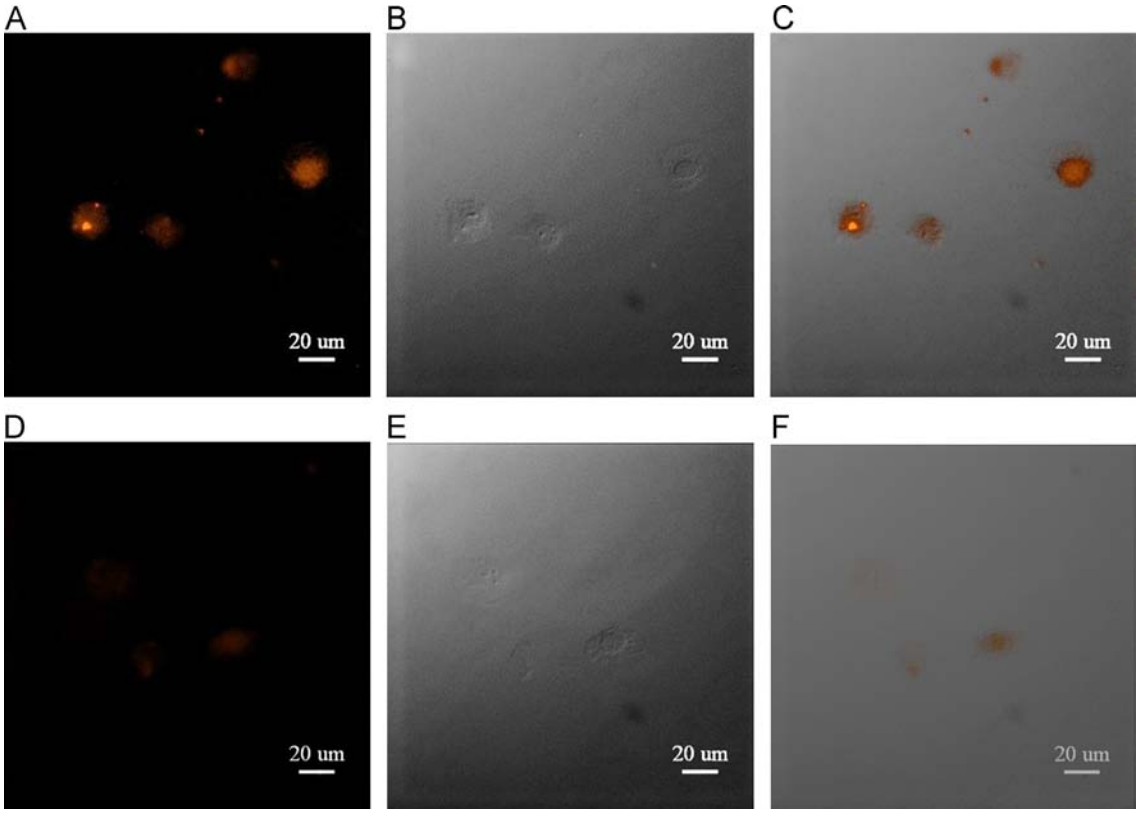

Fig. 8. Fluorescence images of the intracellular $OH^{\bullet}$ of SK-N-SH cells. The upper panels (A–C) show the images of the cells after incubating with DNA-Ag NCs; the lower panels (D–F) show the images of cells incubated with DNA-Ag NCs and then treated with PMA. (A, D) The fluorescence micrographs. (B, E) The images of differential interference contrast (DIC). (C, F) Overlays of fluorescence micrographs and DIC images.

4. Conclusions

In summary, a simple, rapid and label-free sensor has been developed for the essential biological $OH^{\bullet}$ based on the aggregation-induced fluorescence quenching of Ag NCs as a result of the cleavage of template DNA. The DNA-Ag NCs based method circumvents many of the shortcomings of conventional organic fluorophores and demonstrates multifaceted advantages: first of all, the DNA templates used do not require the labor-intensive and expensive modification, and the preparation of DNA-Ag NCs fluorescent indicators is facile, low-cost and accessible to numerous labs; second, the method presented here can be efficiently applied to probe $OH^{\bullet}$ with simple and fast procedure; third, the as-prepared fluorescent probe could be rationally designed according to requirement by modification the template DNA, thus providing feasibility of our proposed approach, especially in the cell recognition and fluorescence detection of intracelluar $OH^{\bullet}$. It is expected that the novel strategy will open new opportunities for the development and design of other extended DNA-Ag NCs systems for fluorescence study, sensing applications and biological imaging in the future.

Acknowledgments

The work was supported by the National Natural Science Foundation of China (Grant nos. 21105044, 21163014, 21265012 and 21265017) and the Program for New Century Excellent Talents in University (NCET-11-1002).

Appendix A. Supplementary material

Supplementary data associated with this article can be found in the online version at http://dx.doi.org/10.1016/j.talanta.2013.09.021.

References

[1] H.R. McLennan, M.D. Esposti, J. Bioenerg. Biomembr. 32 (2000) 153–162.
[2] H. Nohl, A.V. Kozlov, L. Gille, K. Staniek, Biochem. Soc. Trans. 31 (2003) 1308–1311.
[3] H. Wiseman, B. Halliwell, Biochem. J. 313 (1996) 17–29.
[4] J.M. McCord, Science 185 (1974) 529–531.
[5] K. Dobashi, B. Ghosh, J.K. Orak, I. Singh, A.K. Singh, Mol. Cell. Biochem. 205 (2000) 1–11.
[6] M. Nishida, Y. Maruyama, R. Tanaka, K. Kontani, T. Nagao, H. Kurose, Nature 408 (2000) 492–495.
[7] B. Molavi, J.L. Mehta, Curr. Opin. Cardiol. 19 (2004) 488–493.
[8] S. Passi, G. Gianni, M. Cocchi, Prog. Nutr. 6 (2006) 241–256.
[9] A. Manea, E. Constantinescu, D. Popov, M. Raicu, J. Cell. Mol. Med. 8 (2004) 117–126.
[10] M.E. Goetz, A. Luch, Cancer Lett. 266 (2008) 73–83.
[11] V. Afonso, R. Champy, D. Mitrovic, P. Collin, A. Lomri, Joint Bone Spine 74 (2007) 324–329.
[12] B.N. Ames, M.K. Shigenaga, T.M. Hagen, Proc. Natl. Acad. Sci. 90 (1993) 7915–7922.
[13] D.C. Malins, N.L. Polissar, S.J. Gunselman, Proc. Natl. Acad. Sci. 93 (1996) 2557–2563.
[14] A.C. Jacobs, M.J.E. Resendiz, M.M. Greenberg, J. Am. Chem. Soc. 132 (2010) 3668–3669.
[15] S.P. Gieseg, J.A. Simpson, T.S. Charlton, M.W. Duncan, R.T. Dean, Biochemistry 32 (1993) 4780–4786.
[16] M. Tien, B.A. Svingen, S.D. Aust, Arch. Biochem. Biophys. 216 (1982) 142–151.
[17] F. Gerson, W. Huber, Electron Spin Resonance Spectroscopy of Organic Radicals, Wiley-VCH, Weinheim, 2003.
[18] P. Teismann, B. Ferger, Brain Res. 5 (2000) 204–210.
[19] F. Scholz, G. López de Lara González, L. Machado de Carvalho, M. Hilgemann, K. Z. Brainina, H. Kahlert, R.S. Jack, D.T. Minh, Angew. Chem. Int. Ed. 46 (2007) 8079–8081.
[20] Q. Shen, Z. Nie, M. Guo, C.-J. Zhong, B. Lin, W. Li, S. Yao, Chem. Commun. (2009) 929–931.
[21] B. Tang, N. Zhang, Z. Chen, K. Xu, L. Zhuo, L. An, G. Yang, Chem. Eur. J. 14 (2008) 522–528.
[22] M. Liu, Q. Zhang, H. Zhao, S. Chen, H. Yu, Y. Zhang, X. Quan, Chem. Commun. 47 (2011) 4084–4086.
[23] S.E. Page, K.T. Wilke, V.C. Pierre, Chem. Commun. 46 (2010) 2423–2425.
[24] A. Gomes, E. Fernandes, J.L.F.C. Lima, J. Biochem. Biophys. Methods 65 (2005) 45–80.
[25] N. Soh, Anal. Bioanal. Chem. 386 (2006) 532–543.
[26] Y. Manevich, K.D. Held, J.E. Biaglow, Radiat. Res. 148 (1997) 580–591.
[27] G.M. Makrigiorgos, J. Baranowska-Kortylewicz, E. Bump, S.K. Sahu, R. M. Berman, A.I. Kassis, Int. J. Radiat. Biol. 63 (1993) 445–458.
[28] N. Soh, K. Makihara, T. Ariyoshi, D. Seto, T. Maki, H. Nakajima, K. Nakano, T. Imato, Anal. Sci. 24 (2008) 293–296.
[29] L. Yuan, W. Lin, J. Song, Chem. Commun. 46 (2010) 7930–7932.
[30] P. Li, T. Xie, X. Duan, F. Yu, X. Wang, B. Tang, Chem. Eur. J. 16 (2010) 1834–1840.
[31] J. Zheng, P.R. Nicovich, R.M. Dickson, Annu. Rev. Phys. Chem. 58 (2007) 409–431.
[32] H. Xu, K.S. Suslick, ACS Nano 4 (2010) 3209–3214.
[33] W. Guo, J. Yuan, E. Wang, Chem. Commun. (2009) 3395–3397.
[34] Y.-T. Su, G.-Y. Lan, W.-Y. Chen, H.-T. Chang, Anal. Chem. 82 (2010) 8566–8572.
[35] M. Zhang, S.-M. Guo, Y.-R. Li, P. Zuo, B.-C. Ye, Chem. Commun. 48 (2012) 5488–5490.
[36] Z. Huang, F. Pu, Y. Lin, J. Ren, X. Qu, Chem. Commun. 47 (2011) 3487–3489.
[37] J. Sharma, H.-C. Yeh, H. Yoo, J.H. Werner, J.S. Martinez, Chem. Commun. 47 (2011) 2294–2296.
[38] J.T. Petty, B. Sengupta, S.P. Story, N.N. Degtyareva, Anal. Chem. 83 (2011) 5957–5964.
[39] J. Zheng, R.M. Dickson, J. Am. Chem. Soc. 124 (2002) 13982–13983.
[40] Z. Shen, H. Duan, H. Frey, Adv. Mater. 19 (2007) 349–352.
[41] I. Díez, M. Pusa, S. Kulmala, H. Jiang, A. Walther, A.S. Goldmann, A.H.E. Müller, O. Ikkala, R.H.A. Ras, Angew. Chem. Int. Ed. 48 (2009) 2122–2125.
[42] J. Yu, S.A. Patel, R.M. Dickson, Angew. Chem. Int. Ed. 46 (2007) 2028–2030.
[43] X. Le Guével, B. Hötzer, G. Jung, K. Hollemeyer, V. Trouillet, M. Schneider, J. Phys. Chem. C 115 (2011) 10955–10963.
[44] J.T. Petty, J. Zheng, N.V. Hud, R.M. Dickson, J. Am. Chem. Soc. 126 (2004) 5207–5212.
[45] M.L. Neidig, J. Sharma, H.-C. Yeh, J.S. Martinez, S.D. Conradson, A.P. Shreve, J. Am. Chem. Soc. 133 (2011) 11837–11839.
[46] H.-C. Yeh, J. Sharma, J.J. Han, J.S. Martinez, J.H. Werner, Nano Lett. 10 (2010) 3106–3110.
[47] W. Guo, J. Yuan, Q. Dong, E. Wang, J. Am. Chem. Soc. 132 (2010) 932–934.
[48] C.M. Ritchie, K.R. Johnsen, J.R. Kiser, Y. Antoku, R.M. Dickson, J.T. Petty, J. Phys. Chem. C 111 (2007) 175–181.
[49] A.P. Marchetti, A.A. Muenter, R.C. Baetzold, R.T. McCleary, J. Phys. Chem. B 102 (1998) 5287–5297.
[50] W.K. Pogozelski, T.D. Tullius, Chem. Rev. 98 (1998) 1089–1108.
[51] D.F. Bishop, G. Stern, M. Fleischman, L.S. Marshall, Ind. Eng. Chem. Proc. Des. Dev. 7 (1968) 110–117.
[52] S.A. Patel, M. Cozzuol, J.M. Hales, C.I. Richards, M. Sartin, J.-C. Hsiang, T. Vosch, J.W. Perry, R.M. Dickson, J. Phys. Chem. C 113 (2009) 20264–20270.
[53] P. Pyykkö, Angew. Chem. Int. Ed. 43 (2004) 4412–4456.
[54] G.A. Miller, J. Phys. Chem. 82 (1978) 616–618.
[55] M. Rosa, R. Dias, M. da Graça Miguel, B. Lindman, Biomacromolecules 6 (2005) 2164–2171.
[56] Y. Sang, L. Zhang, Y.F. Li, L.Q. Chen, J.L. Xu, C.Z. Huang, Anal. Chim. Acta 659 (2010) 224–228.
[57] Y. Luo, E.S. Henle, S. Linn, J. Biol. Chem. 271 (1996) 21167–21176.